Cancer Research

Hypoxia-Induced Downregulation of DUSP-2 Phosphatase Drives Colon Cancer Stemness

Pei-Chi Hou[1], Yo-Hua Li[1], Shih-Chieh Lin[2], Shau-Chieh Lin[3], Jenq-Chang Lee[3], Bo-Wen Lin[3], Jing-Ping Liou[4], Jang-Yang Chang[5], Ching-Chuan Kuo[6], Yi-Min Liu[4], H. Sunny Sun[1,7], and Shaw-Jenq Tsai[1,2]

Abstract

Cancer stem-like cells (CSC) evolve to overcome the pressures of reduced oxygen, nutrients or chemically induced cell death, but the mechanisms driving this evolution are incompletely understood. Here, we report that hypoxia-mediated downregulation of the dual specificity phosphatase 2 (DUSP2) is critical for the accumulation of CSC in colorectal cancer. Reduced expression of DUSP2 led to overproduction of COX-2–derived prostaglandin E_2, which promoted cancer stemness via the EP2/EP4 signaling pathways. Genetic and pharmacological inhibition of PGE_2 biosynthesis or signal transduction ameliorated loss-of-DUSP2–induced tumor growth and cancer stemness. Genome-wide profile analysis revealed that genes regulated by DUSP2 were similar to those controlled by histone deacetylase. Indeed, treatment with novel histone deacetylase inhibitors abolished hypoxia-induced DUSP2 downregulation, COX-2 overexpression, cancer stemness, tumor growth, and drug resistance. Our findings illuminate mechanisms of cancer stemness and suggest new cancer therapy regimens. *Cancer Res; 77(16); 4305–16. ©2017 AACR.*

Downloaded from http://aacrjournals.org/cancerres/article-pdf/77/16/4305/2753507/4305.pdf by guest on 26 August 2022

Introduction

Cancer stem-like cells (CSC) or tumor-initiating cells comprise a small population of tumor-forming, self-renewing cancer cells within a tumor. The high ability of self-renewal and epithelial–mesenchymal transition in CSCs results in resistance to chemotherapy and cancer metastasis, and often leads to poor prognosis (1). Accumulated data demonstrate that CSCs can be isolated from solid tumors such as colon, ovary, lung, prostate, breast, and pancreas (2–7). The formation of CSCs may be due to accumulated mutations in somatic stem cells during neoplasia (8) or de-differentiation caused by increasing SOX2 expression (9), Wnt signaling (10), TGF-β stimulation (11), or hypoxic stress (12).

Hypoxia is an intrinsic stress occurring within the tumoral microenvironment due to the fast growth of cancer cells, poorly formed neoangiogenic blood vessels, or even chemotherapy-induced ischemia. Since oxygen can only diffuse to about 100 to 200 μm away from a capillary (13, 14), cancer cells encounter hypoxic stress at a very early stage during cancer development. In the later stage of cancer progression, although hypoxia can induce neoangiogenesis, the newly formed microvessels within the tumor are usually leaky and not fully functional (15). The oxygen transporting ability of microvessels in tumor tissue is not as efficient as that of mature blood vessels in normal tissues; therefore, cancer cells are likely to encounter hypoxic stress. Under such hypoxic stress, cancer cells need to acquire the ability to survive under conditions of less oxygen and nutrients, to increase mobilizing capacity, and to increase resistance to the highly acidic microenvironment. The slow cycling and pluripotent CSCs possess a better survival advantage in such an unfavorable hypoxic microenvironment. Therefore, it is likely that hypoxic stress may drive some cancer cells to become CSCs. However, how hypoxia promotes CSC formation remains largely uncharacterized.

Hyperactivation of ERK was observed in $CD133^{high}$ primary cells derived from patients with colorectal cancer when compared to their $CD133^{low}$ counterparts (16). In contrast, inactivation of ERK signaling leads to massive cell death and differentiation in human embryonic stem cells (17). These results suggest that activation of ERK plays an important role in stemness maintenance. Dual specificity phosphatase-2 (DUSP2) is a nuclear-specific phosphatase, which predominantly inactivates ERK and p38 by direct dephosphorylation of phosphothreonine and phosphotyrosine residues (18). Previous studies reported that DUSP2 is involved in P53-induced cell apoptosis (19), inflammatory response (20), and angiogenesis (21, 22). Our previous study showed that DUSP2 is markedly reduced in many solid tumors compared with their normal counterparts, and reduction of DUSP2 leads to prolonged ERK phosphorylation and increased drug resistance

[1]Institute of Basic Medical Sciences, College of Medicine, National Cheng Kung University, Tainan, Taiwan. [2]Department of Physiology, College of Medicine, National Cheng Kung University, Tainan, Taiwan. [3]Department of Surgery, College of Medicine, National Cheng Kung University, Tainan, Taiwan. [4]School of Pharmacy, College of Pharmacy, Taipei Medical University, Taipei, Taiwan. [5]Department of Internal Medicine, College of Medicine, National Cheng Kung University, Tainan, Taiwan. [6]Institute of Biotechnology & Pharmaceutical Research, National Health Research Institutes, Zhunan, Taiwan. [7]Institute of Molecular Medicine, College of Medicine, National Cheng Kung University, Tainan, Taiwan.

Note: Supplementary data for this article are available at Cancer Research Online (http://cancerres.aacrjournals.org/).

P.-C. Hou and Y.-H. Li are co-first authors for this article.

Corresponding Author: Shaw-Jenq Tsai, National Cheng Kung University, 1 University Road, Tainan 70101, Taiwan. Phone: 886-6-235-3535, ext. 5426; Fax: 886-6-236-2780; E-mail: seantsai@mail.ncku.edu.tw

doi: 10.1158/0008-5472.CAN-16-2990

©2017 American Association for Cancer Research.

(23). However, the underlying mechanisms responsible for loss-of-DUSP2–mediated cancer progression remain untested.

Herein, we hypothesize that DUSP2, a potent nuclear phosphatase that directly inactivates ERK, may serve as a tumor suppressor that represses the ability of cancer stemness and progression. Loss-of-DUSP2 in cancer cells may thus contribute to the enrichment and/or maintenance of CSCs. This study was designed to unravel the underlying mechanism of hypoxia-triggered, DUSP2-mediated cancer stemness and to explore the possibility of designing novel drugs for better intervention.

Materials and Methods

Isolation of primary colorectal cancer cells

Primary colorectal cancer tissues were mechanically and enzymatically disaggregated into a single-cell suspension. In brief, freshly resected tissue was cut into small pieces using a cross scalpel technique and then incubated with 5% collagenase type IV and DNase I at 37°C for 2 hours with gentle agitation. Undigested tissue was removed by passing through cell strainers (Falcon) and red blood cells were lyzed by incubating with hypotonic solution. Cells were further disaggregated by pipetting and serial filtration through 40-μm and 80-μm meshes (Sigma-Aldrich). Cells were then washed with calcium- and magnesium-free Hank's balanced salt solution and centrifuged at 1,000 rpm for 2 to 3 minutes. Both Hank's solution and culture medium (DMEM/F12) contained 1X Antibiotic–Antimycotic solution (Gibco, BRL) to prevent bacterial and fungal contamination. The isolated primary colorectal cancer cells were confirmed by the immunofluorescence staining using antibodies against pan-keratin (epithelial-marker) and vimentin (mesenchymal marker). This study was approved by Institutional Review Board at the National Cheng Kung University Medical Center and informed consent was obtained from each patient.

Cell culture and treatments

Colorectal cancer cell lines were purchased from Bioresource Collection and Research Center (Hsinchu City, Taiwan) between 2012 and 2015. Colorectal cancer cell lines, HCT116, HT29, were cultured in McCoys' 5A medium, whereas LS123 and Caco-2 cells were cultured in MEM medium. Primary colorectal cancer cells, xenograft HCT116 cells, and HeLa cells were cultured in DMEM/F12 medium. Cells were routinely checked for mycoplasma contamination by using Hoechst staining and PCR. All cell lines were authenticated by Center for Genomic Medicine at National Cheng Kung University (HCT116, HT-29, and LS123) and by Mission Biotech (HT-29 and Caco-2). All media were supplemented with 10% FBS, 2-mmol/L L-Glutamax, and antibiotics. Stable shRNA knockdown clones or inducible expression clones were kept under the selected antibiotics, puromycin, hygromycin B, or G418, respectively. For hypoxia treatment, cells were cultured in a humidified incubator (Thermo Scientific) filled with 94% N_2, 5% CO_2, and 1% O_2 at 37°C for 24 or 48 hours.

Construction of inducible expression system

The GFP or DUSP2-GFP cDNA was cloned into an all-in-one Tet-on vector system (pAS4.1w.Ppuro-aOn). Virus-associated plasmids were transformed into Stbl3 (Yeastern Biotech) bacteria for plasmid amplification. Inducible GFP and DUSP2-GFP were packaged as particle for virus infection. After being cultured in the presence of puromycin for two months, stable clones of inducible DUSP2-GFP (iDUSP2-GFP) and inducible GFP (iGFP) were established.

Tumorsphere formation assay

Cancer cells were plated onto a 96-well ultra-low attachment plate and incubated for 10 to 14 days in stem cell medium. The supplied medium was serum-free DMEM/F12 containing recombinant human EGF (20 ng/mL), basic FGF (20 ng/mL), LIF (10 ng/mL), and insulin (5 μg/mL). Spheroids greater than 50 μm were counted. A second sphere formation assay was performed by trypsinizing and dissociating cells of the first spheroid. For spheroid cell differentiation assay, spheroids were placed on a regular culture dish and cultured in the presence of DMEM/F12 supplemented with 10% FBS.

Flow cytometry

Cells were resuspended in a small volume of cold flow cytometry buffer, and then directly stained with various fluorescence-conjugated antibodies such as CD44-APC (Miltenyi Biotec, Bergisch Gladbach, Germany), CD133/2-PE (Miltenyi Biotec), and CD24-PE (Beckman Coulter Taiwan Inc.). After washing off excess unbound antibodies, cells were resuspended in 500 μL cold buffer and passed through a falcon tube with a cell strainer cap. Cell population calculation was performed by flow cytometer CantoII, and data were analyzed using the FlowJo software.

Isolation of $CD133^+$ cells

Cells were labeled with the magnetic CD133 MicroBead Kit (Miltenyi Biotec) at 4°C for 20 minutes, then washed by cold flow buffer once, and resuspended in 5 mL cold flow buffer. Cell sorting was performed by using an AutoMACS separator. The $CD133^-$ and $CD133^+$ were collected separately in 15 mL centrifuge tubes containing 5 mL 10% FBS culture medium.

Prostaglandin E_2 enzyme-linked immunoassay

Treated cancer cells were cultured in a suitable medium with 1% FBS for 48 hours. Then, conditioned media were collected. The concentrations of PGE_2 in conditioned media were analyzed by monoclonal PGE_2 enzyme immunoassay kit (Cayman) according to the manufacturer's protocol as previously described (24).

Soft agar assay

Equal volumes of 1.2% agar solution and 2X McCoy's 5A medium were mixed in a sterile, pre-warmed tube by inversion. Fifty μL of the mixture were transferred immediately to each well of a 96-well sterile flat-bottom microplate. When the bottom layer had gelled, 1×10^4 cells were plated in a 6-well plate and mixed with 0.35% agarose in 2 mL to create a soft agar top layer. After solidification, 2 ml McCoy's 5A medium containing 10% FBS was added on top of the agar. Cultured medium was replaced with a fresh one every 4 days. Colonies were stained with 0.025% crystal violet and counted on day 14.

Immunofluorescence staining

Cells were fixed in 4% para-formaldehyde for 20 minutes. After washing with 1X PBS buffer twice, cells were permeabilized with 0.5% Triton X-100 for 5 minutes and then washed

Downloaded from http://aacrjournals.org/cancerres/article-pdf/77/16/4305/2753507/4305.pdf by guest on 26 August 2022

with 1X PBS buffer for 5 minutes. Samples were blocked by blocking buffer (Superblock) for 1 hour and hybridized with first antibodies overnight at 4°C. Fluorochrome-488–conjugated goat anti-mouse IgG (H+L), Alexa Fluor 594 phalloidin (direct conjugated antibody, 1:1,000), and Hoechst (1:5,000) were incubated with sample for 1 hour at room temperature in the dark. Images were taken by a multi-photon confocal microscope (FV1000MPE).

Cell migration and invasion assay

Cells in 100 μL culture medium supplemented with 10% FBS were plated in the inner-well in a 24-well plate format. The outer chamber was filled with 700 μL culture media supplemented with 10% FBS. After 24 hours, medium in the inner-well was replaced with serum-free medium. In the invasion assay, an extra layer of Matrigel was coated and cells were allowed to invade for 24 hours. In the migration assay, the incubation time was 24 hours for Caco2 cells and 8 hours for HCT116 cells. Cells were then fixed with 3.7% formaldehyde in 1X PBS, permeabilized with 0.5% Triton X-100, and stained with hematoxylin solution. Non-invaded or non-migrated cells on the top side of the Transwell were scraped off by means of a cotton swab. Ten photos were taken by color microscope for cell number counting.

Reverse transcriptase quantitative PCR and Western blotting

Total RNA from cell cultures was harvested by TRIsure reagent (Invitrogen Life Technologies, Inc.) according to the manufacturer's instructions. Gene expressions were quantified by ABI StepOne plus thermocycler. The standard protocol for Western blotting was performed (23). The DUSP2 and OCT4 antibodies were purchased from Santa Cruz Biotechnology Inc. The COX-2 antibody was purchased from Cayman. The GFP, Snail, E-cad, p-ERK, T-ERK, p-p38, T-p38, Nanog, and SOX2 antibodies were purchased from Cell Signaling Technology. Primary antibody dilution factors were as follows: DUSP2, 1:200; β-actin, 1:10,000; Nanog, 1:1,000; SOX2, 1:1,000; for other antibodies: 1:2,000.

Xenograft mouse model

Various kinds of cancer cells were suspended in 100 μL of 1X PBS and inoculated subcutaneously in the hind flank of male SCID mice (6- to 8-weeks-old, from the Animal Center at the College of Medicine, National Cheng Kung University). The mice were housed in barrier facilities on a 12 hours light–dark cycle with food and water available ad libitum. All procedures were performed in accordance with the Guidelines for the handling of laboratory animals by the National Cheng Kung University Animal Center. After the tumors grew to about 50 mm^3, the mice were randomly assigned into experimental or control groups and subjected to specific treatments according to the protocols. Tumor sizes were measured and tumor volume was calculated according to the formula: $0.52 \times (\text{length} \times \text{width} \times \text{height})$.

Novel histone deacetylase inhibitors

MPT0B369 {3-[1-Benzenesulfonyl-1H-pyrrolo(2,3-b)pyridin-5-yl]-N-hydroxy-acrylamide} and MPT0B390 {N-Hydroxy-3-[1-(4-methoxy-benzenesulfonyl)-2,3-dihydro-1H- pyrrolo(2,3-b) pyridin-5-yl]-acrylamide} are the novel N-hydroxyacrylamide-derived HDAC inhibitors with the 7-azaindole and 7-azaindoline core, respectively, which were synthesized at Dr. Jing-Ping Liou's laboratory (Taipei Medical University, Taipei, Taiwan). The detailed synthetic methods and structure and activity relationship will be published elsewhere.

HDACs inhibition assays

Method A. The IC_{50} values of HDAC inhibitors were determined by a fluorimetric histone deacetylase assay following the manufacturer's instructions. For the pan-HDAC assay, HeLa nuclear extracts were used as a source of histone deacetylase (BioVision Inc.). Briefly, 0.25 mg of protein per mL of HeLa nuclear extract was incubated for 30 minutes with the test compound and 500 μmol/L HDAC kit substrate [Boc-Lys(Ac)-AMC]. The reaction was stopped by adding lysine developer, and then the mixture was incubated for 30 minutes. The fluorescence generated by the deacetylated substrate was measured with a SpectraMax M5 multidetection microplate reader (Molecular Devices) at a wavelength of 360 nm and an emission wavelength of 460 nm. The IC_{50} is determined as the concentration of compound that results in 50% reduction of HDAC activity increase in control wells during the compound incubation. The reaction was done in triplicate for each sample. Each point represents the mean ± SD of replicates.

Method B. HDAC1, HDAC2, and HDAC6 enzyme inhibition assays were conducted by the Reaction Biology Corporation (www.reactionbiology.com). The substrate for HDACs 1, 2, and 6 is a fluorogenic peptide derived from p53 residues 379–382 [RHKK(Ac)]. Compounds were dissolved in DMSO and tested in 10-dose IC_{50} mode with 3-fold serial dilution starting at 10 μmol/L.

In vivo test of novel anticancer drugs

HCT116 cells (5×10^5) suspended in 100 μL of 1× PBS were inoculated subcutaneously in the hind flank of 6- to 8-week-old male SCID mice. After the tumors reached about 25 mm^3, the mice were randomly assigned into experimental or control groups. Synthetic MPT0B369 (B369), MPT0B390 (B390) compounds, and suberoylanilide hydroxamic acid (SAHA) were dissolved in 10% N-Methyl-2-pyrrolidone/90% PEG300 (Sigma). Mice received vehicle, 25 mg/kg MPT0B369, 12.5 mg/kg MPT0B369, 25 mg/kg MPT0B390, 12.5 mg/kg MPT0B390, or 25 mg/kg SAHA, respectively, by oral gavage with flexible feeding tubes 5 days/week for 2 consecutive weeks. Tumor sizes were measured every 3 days and tumor volumes were calculated by the equation of $0.52 \times (\text{length} \times \text{width} \times \text{height})$. Mice were sacrificed 3 days after the last treatment and tumors were excised.

Statistical analysis

The data were expressed as means ± standard errors of the mean and were analyzed by either the two-tailed Student *t* test (for two groups) or one-way ANOVA (for three or more groups) using GraphPad Prism 5.0 (GraphPad Software, Inc.). Post-test analysis was performed using Tukey's multiple comparison. Tumor-free data were analyzed using the Kaplan–Meier method and compared by log-rank test. A *P* value less than 0.05 was considered statistically significant.

Downloaded from http://aacrjournals.org/cancerres/article-pdf/77/16/4305/2753507/4305.pdf by guest on 26 August 2022

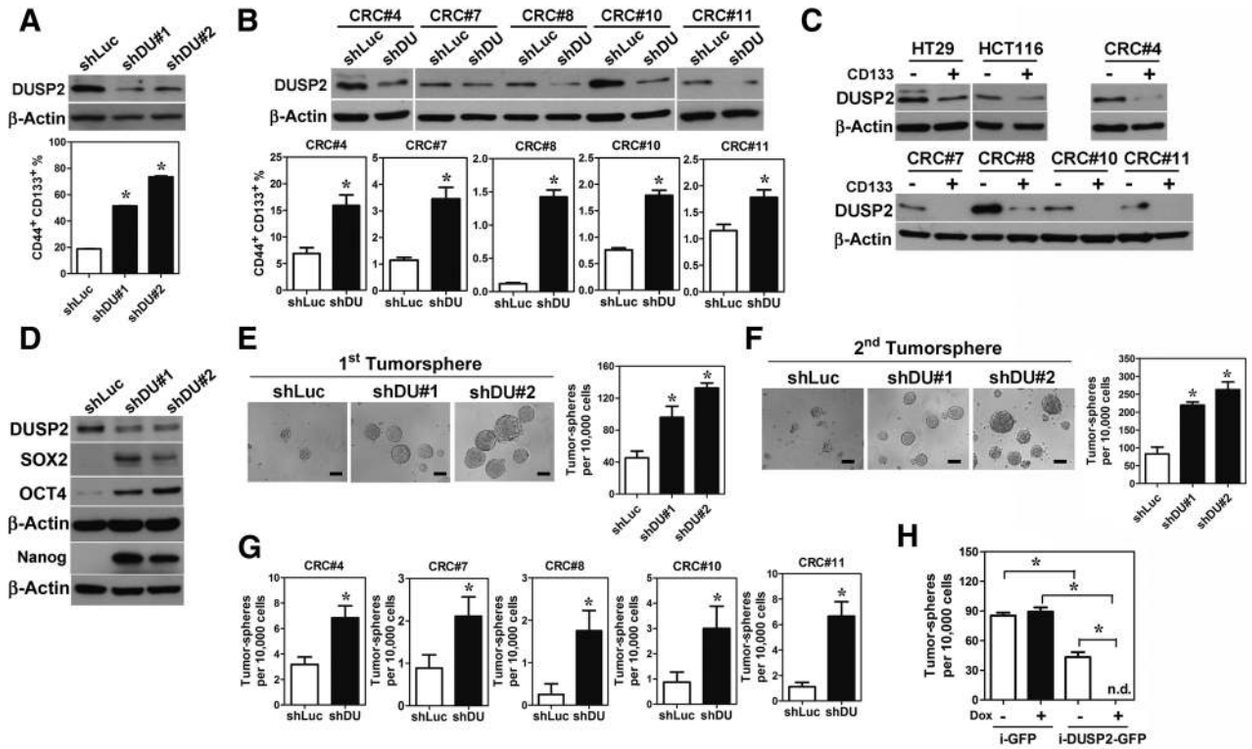

Figure 1.

DUSP2 negatively regulates cancer stemness. **A,** The percentage of $CD44^+/CD133^+$ population in control (shLuc) and DUSP2 knockdown (shDU#1 and shDU#2) HCT116 cells. Data shown are the mean ± SEM of three independent experiments using different batches of cells. **B,** The percentage of $CD44^+/CD133^+$ population in primary colorectal cancer cells without (shLuc) or with DUSP2 knockdown (shDU). CRC, colorectal cancer. CRC#, different patient. Data shown are the mean ± SEM of three independent experiments using different batches of cells. **C,** Levels of DUSP2 in $CD133^+$ and $CD133^-$ cancer cells. HT29 and HCT116 are colorectal cancer cell lines while CRC# indicates primary colorectal cancer cells isolated from different patients. **D,** Representative Western blots showed levels of DUSP2, OCT4, Nanog, SOX2, and β-actin in HCT116 cells without and with DUSP2 knockdown. **E** and **F,** Tumorsphere formation abilities of HCT116 cells without (shLuc) and with (shDU#1 and shDU#2) DUSP2 knockdown. The spheroids in first tumorsphere (**E**) were dissociated and cells were used for second round of tumorsphere formation assay (**F**). Tumorsphere with diameter greater than 50 μm was counted. Data shown are the mean ± SEM of three independent experiments using different batches of cells. **G,** Tumorsphere formation abilities in primary colorectal cancer cells isolated from different patients (CRC#) without (shLuc) and with (shDU) DUSP2 knockdown. **H,** Tumorsphere formation ability in HCT116 cells carrying inducible minigenes encoding for GFP or DUSP2-GFP without (−) and with (+) doxycycline induction. DUSP2 overexpression was induced by 2 μg/mL doxycycline. n.d., not detected. *, $P < 0.05$.

Results

Loss-of-DUSP2 promotes cancer stemness

To characterize the relationship between DUSP2 and cancer stemness, we knocked down DUSP2 in cancer cells and examined the expression of cancer stemness markers as well as the tumorsphere formation ability. Knockdown of DUSP2 enriched the CSC population in several cancer cell lines (Fig. 1A and Supplementary Fig. S1A and S1B) and primary colorectal cancer cells (Fig. 1B and Supplementary Fig. S1C). This result was mirrored by the observation that the level of DUSP2 was significantly decreased in $CD133^+$ colorectal cancer cells compared with $CD133^-$ cells (Fig. 1C).

Consistent with the cell-surface marker results, the stemness-maintenance genes such as *OCT4*, *NANOG*, and *SOX2* (Fig. 1D and Supplementary Fig. S1B) and tumorsphere formation ability (Fig. 1E and Supplementary Fig. S1C) were significantly increased in DUSP2-knockdown cancer cell lines. In addition, these CSCs can differentiate when plated on a solid surface and re-form a tumorsphere again when cultured in an ultra-low plate (Fig. 1F and Supplementary Fig. S1D and S1E). The sphere-forming ability was greater in the DUSP2-knockdown cells compared with control cells (Fig. 1F and Supplementary Fig. S1E). Again, DUSP2-knockdown primary colorectal cancer cells exerted better colonosphere forming ability than control cancer cells (Fig. 1G). Results from a limited dilution assay showed that tumorsphere-forming ability increased by 2.5- to 4.8-fold in DUSP2-knockdown primary colorectal cancer cells (Supplementary Table S1). In contrast, the forced expression of DUSP2 in cancer cells markedly inhibited tumorsphere formation (Fig. 1H). Taken together, these data demonstrate that DUSP2 plays a critical role in the regulation of cancer stemness, and that a dysfunction of DUSP2 promotes the self-renewal ability of cancer cells.

DUSP2 negatively regulates cancer malignancy

Next, we tested whether loss-of-DUSP2 contributes to major pathological processes associated with cancer malignancy, including epithelial–mesenchymal transition, migration, invasion, and anchorage-independent growth. Results demonstrate that knockdown of DUSP2 induced the expression of mesenchymal marker, Snail (Supplementary Fig. S2A) and inhibited epithelial

Downloaded from http://aacrjournals.org/cancerres/article-pdf/77/16/4305/2753507/4305.pdf by guest on 26 August 2022

marker, E-cadherin (Supplementary Fig. S2B). Concomitantly, the migration and invasion abilities were markedly enhanced in cancer cells with DUSP2 knockdown (Supplementary Fig. S2C and S2D). Knockdown of DUSP2 also increased anchorage-independent growth ability on soft agar (Supplementary Fig. S2E). In contrast, forced expression of DUSP2 reduced the expression of mesenchymal and stemness markers, increased epithelial marker, and inhibited cell migration (Supplementary Fig. S2F and S2G).

DUSP2 inhibits COX-2-derived PGE_2 production

To investigate the underlying mechanisms responsible for DUSP2-mediated cancer stemness, we reanalyzed the microarray data, which was derived from DUSP2-overexpressed HeLa cells, to profile downstream genes regulated by DUSP2 (GEO submission number GSE66656). Our data indicated that the levels of genes involved in cancer stemness and prostaglandin (PG) synthesis were inversely correlated with DUSP2 (Supplementary Fig. S3A). Because PGE_2 has been shown to increase embryonic stem cell population (25, 26), *COX-2* was selected for further investigation. Our data showed that knockdown of DUSP2 induced COX-2 expression and PGE_2 production (Fig. 2A), whereas forced expression of DUSP2 repressed COX-2 expression and PGE_2 production (Fig. 2B). Similarly, knockdown of DUSP2 led to COX-2 upregulation and PGE_2 overproduction in primary colorectal cancer cells (Fig. 2C and D).

Next, we tested whether loss-of-DUSP2-induced cancer stemness is mediated by PGE_2. Treatment with PGE_2 enhanced colonosphere formation in cancer cell lines and primary colorectal cancer cells (Fig. 2E and Supplementary Fig. S3B), whereas pretreatment with PGE_2 receptor antagonists, AH6809 (EP2 antagonist) and L161982 (EP4 antagonist), abolished DUSP2-knockdown-induced tumorsphere formation (Fig. 2F). The inhibition of tumorsphere formation by EP receptor antagonists is not due to cytotoxicity, as treatment with AH6809 and L161982 did not affect cell viability even at a higher dose (Supplementary Fig. S3C).

Hypoxia-induced COX-2 expression is mediated by downregulation of DUSP2

Because loss-of-DUSP2 results in COX-2 upregulation and the expression of DUSP2 in many cancers is inhibited by hypoxia (23), we sought to determine whether hypoxia is a driving force

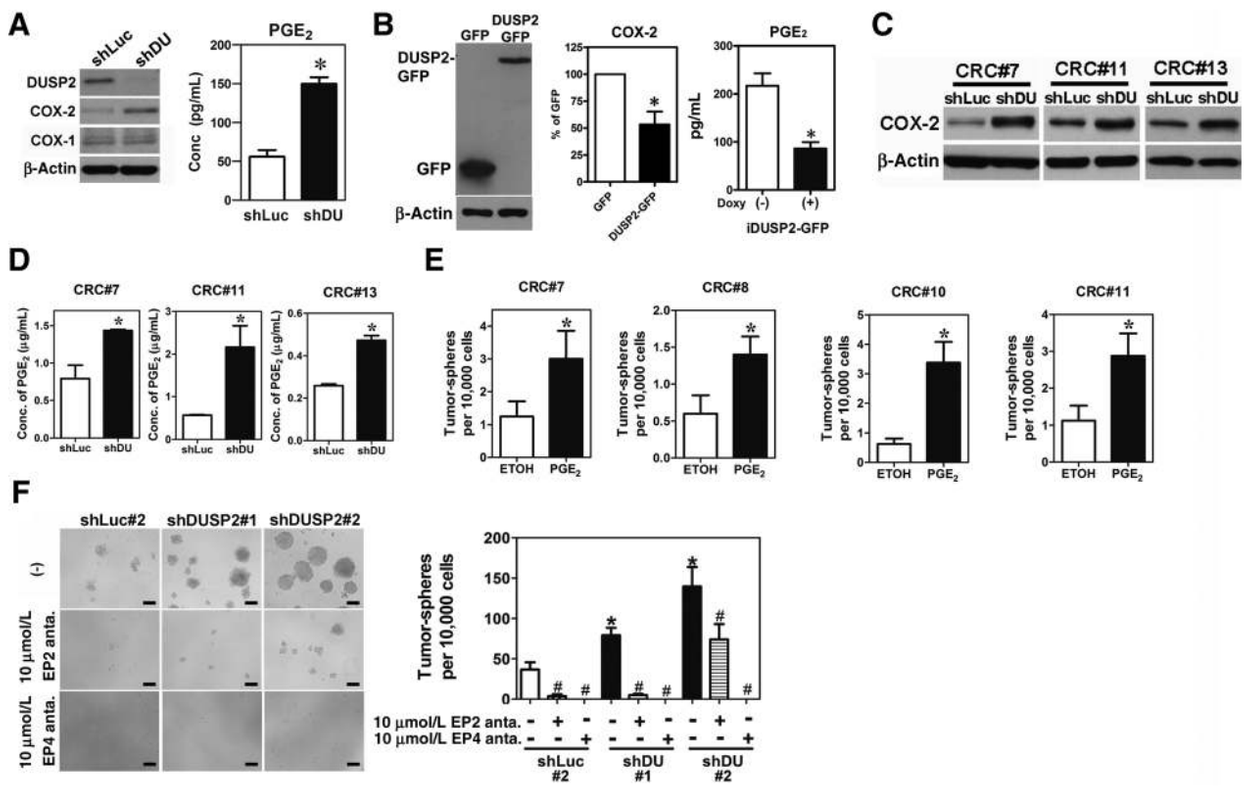

Figure 2.

DUSP2 controls CSCs via COX-2-derived PGE_2 production. **A,** Knockdown of DUSP2 induces COX-2 expression (left) and PGE_2 production (right). Data show results from four independent experiments using different batches of HCT116 cells. **B,** Induction of DUSP2 in HCT116 cells inhibits COX-2 expression (left and middle) and reduces PGE_2 production (right). Data shown are the mean ± SEM of four independent experiments using different batches of cells. **C** and **D,** Knockdown of DUSP2 in primary colorectal cancer cells induces COX-2 expression (**C**) and PGE_2 production (**D**). Data shown are the mean ± SEM of three independent experiments using different batches of primary colorectal cancer cells. Different colorectal cancer (CRC) number represents primary colorectal cancer cells derived from different patient. **E,** Treatment with PGE_2 increases tumorsphere formation ability in primary colorectal cancer cells. Data shown are the mean ± SEM of three independent experiments using different batches of cells. **F,** Treatment with EP2 and EP4 receptor antagonists (EP2 anta and EP4 anta) abolished loss-of-DUSP2-induced tumorsphere formation ability in HCT116 cells. Data (right) shown are the mean ± SEM of four independent experiments using different batches of cells. *, $P < 0.05$; #, $P < 0.05$ compared with the no antagonist treated group.

Downloaded from http://aacrjournals.org/cancerres/article-pdf/77/16/4305/2753507/4305.pdf by guest on 26 August 2022

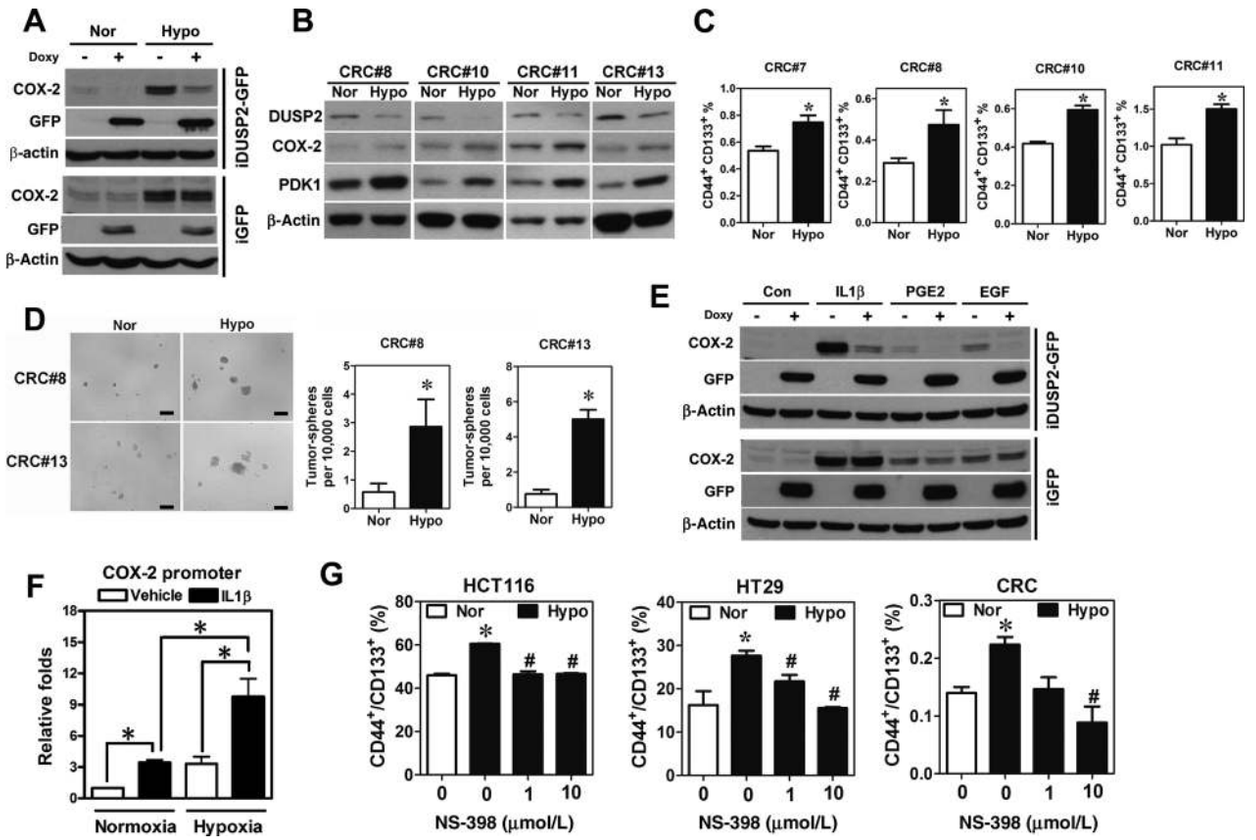

Figure 3.

Hypoxia-mediated DUSP2 downregulation results in COX-2 overexpression. **A,** Representative Western blot analysis shows induction of DUSP2 expression abolished hypoxia-induced COX-2 expression in cancer cell line. HCT116 cells were transfected with inducible GFP (iGFP) or DUSP2-GFP (iDUSP2-GFP) minigenes and stable lines of cells were selected. Doxy (+), addition of doxycycline (2 μg/mL) to induce the expression of DUSP2-GFP (top) or GFP (bottom). **B,** Inhibition of DUSP2 by hypoxia induces COX-2 expression in primary colorectal cancer cells (CRC). Pyruvate dehydrogenase kinase-1 (PDK1) was used as positive control of hypoxic effect. **C** and **D,** Hypoxia treatment increases $CD44^+/CD133^+$ cell population (**C**) and tumorsphere formation ability (**D**) in primary colorectal cancer cells. **E,** Representative images show induction of DUSP2 (top) but not GFP (bottom) abolishes COX-2 upregulation by different stimulators. Cells were incubated with 2 μg/mL doxycycline for 24 hours and then treated with 1 ng/mL IL1β, 10 μmol/L PGE_2, or 100 ng/mL EGF for 12 hrs. **F,** Promoter activity of COX-2 in cancer cells cultured under normoxia or hypoxia in the absence (vehicle) or presence of IL1β (1 ng/mL) for 24 hours. Data shown are the mean ± SEM of three independent experiments using different batches of cells; *, $P < 0.05$. **G,** HCT116, HT29, and primary colorectal cancer cells were cultured under normoxia, hypoxia, or hypoxia plus 1 or 10 μmol/L NS-398 for 24 hours and subjected to flow cytometry analysis of $CD44^+/CD133^+$ cell population. Data shown are the mean ± SEM of three independent experiments using different batches of cells. *, $P < 0.05$ compared with the normoxia group; #, $P < 0.05$ compared with hypoxia without the NS-398–treated group.

for aberrant COX-2 expression in cancer cells. Results demonstrated that hypoxia-induced COX-2 mRNA and protein expressions could be abrogated by addition of doxycycline to induce the expression of DUSP2 (Fig. 3A and Supplementary Fig. S4A and S4B). Time course results revealed that hypoxia-suppressed DUSP2 expression preceded COX-2 upregulation (Supplementary Fig. S4C). Similarly, treatment of primary colorectal cancer cells with hypoxia induced COX-2 expression (Fig. 3B). Meta-analysis of a microarray dataset (E-MTAB-990; ref. 27), which collected gene-expression information from 688 colorectal cancer patients, also demonstrated that the level of *DUSP2* is inversely correlated with *HIF-1α* and *COX-2* (Supplementary Fig. S4D and Supplementary Table S2). Consistent with these findings, treatment of primary colorectal cancer cells with hypoxia increased the $CD44^+/CD133^+$ cell population, and also promoted tumorsphere formation (Fig. 3C and D).

As the tumor microenvironment contains elevated levels of cytokines and growth factors, we aimed to test whether downregulation of DUSP2 by hypoxia would increase the susceptibility of the *COX-2* gene to stimulators presented in the tumor microenvironment. Treatment with IL1β, PGE_2, and epidermal growth factor (EGF), three known factors that are elevated in the tumor microenvironment, induced COX-2 expression, whereas pre-induction of DUSP2, but not GFP, by doxycycline attenuated IL1β, PGE_2, and EGF-induced COX-2 expression (Fig. 3E). A promoter activity assay demonstrated that increased basal and IL1β–induced COX-2 expression by hypoxia is regulated at the transcriptional level (Fig. 3F). Next, we determined whether COX-2 is important for hypoxia-induced cancer stemness. Colorectal cancer cell lines (HCT116 and HT29), as well as primary colorectal cancer cells, were treated with hypoxia in the presence or absence of selective COX-2 inhibitor, NS-398, and then the $CD44^+/CD133^+$ cell populations were quantified by flow cytometry. Results showed that treatment with NS-398 abolished the hypoxia-induced an increase of the $CD44^+/CD133^+$ cell population (Fig. 3G). Taken together, these data demonstrate

Downloaded from http://aacrjournals.org/cancerres/article-pdf/77/16/4305/2753507/4305.pdf by guest on 26 August 2022

that loss-of-DUSP2 under hypoxic stress increases *COX-2* gene susceptibility to proinflammatory cytokine stimulation and that overexpression of COX-2 in cancer cells is critical for increasing cancer stemness.

COX-2 mediates loss-of-DUSP2–induced tumor growth and cancer stemness

The *in vitro* results were recapitulated by *in vivo* study, as the xenografted data showed that tumors that arose from DUSP2 knockdown cells grew faster, expressed more COX-2, possessed greater colonosphere forming ability, and had a larger CSC subpopulation (Fig. 4A–D). Inoculation with a number of different cancer cells on the hind of mice showed that loss-of-DUSP2 not only increased the incidence and accelerated tumor growth (Fig. 4E and Supplementary Fig. S5), but also enriched the population of CSCs *in vivo* (Supplementary Table S3).

We next tested whether inhibiting COX-2 expression and/or activity would attenuate loss-of-DUSP2–induced tumor progression. Knockdown of DUSP2 led to enhanced tumor growth while administration of NS-398, to inhibit COX-2 activity, led to attenuated growth of the tumor induced by DUSP2 knockdown (Fig. 5A). Consistent with this result, the levels of stemness markers, invasion ability, and anchorage-independent growth ability were reduced in DUSP2/COX-2 double knockdown cells (Fig. 5B–D). Tumorspheres, tumor incidence, and tumor mass were markedly reduced in mice inoculated with shDUSP2/shCOX-2 cells compared with those inoculated with shDUSP2 cells (Fig. 5E–G and Supplementary Table S4). The cancer cells were isolated from xenografted tumors and re-injected into recipients to start the second run of the xenograft assay. Again, shDUSP2-increased tumorsphere, tumor incidence, and tumor mass were reduced when COX-2 was knocked down (Fig. 5H–J). Taken together, these data indicate that the COX-2 expression induced by hypoxia-mediated loss-of-DUSP2 is a critical factor in promoting tumor growth and cancer stemness during cancer progression.

HDACi reverses hypoxia-mediated DUSP2 downregulation and COX-2 upregulation

Because hypoxia-mediated DUSP2 downregulation results in PGE_2 overproduction and cancer malignancy, disrupting such a signaling pathway seems to be a reasonable approach for cancer therapy. To accomplish this goal, we analyzed our DUSP2-overexpressed microarray data by cross-referencing with the connectivity map (28). Results showed that the gene signatures in HDACi-treated cells were positively correlated with those of DUSP2-overexpressed cells (Supplementary Table S5), suggesting that treatment with HDACi may reverse loss-of-DUSP2 effects. To test this hypothesis, cells were treated with different doses of known HDACi under hypoxia and the results demonstrated that hypoxia-inhibited DUSP2 expression was reversed by the addition of SAHA, trichostatin

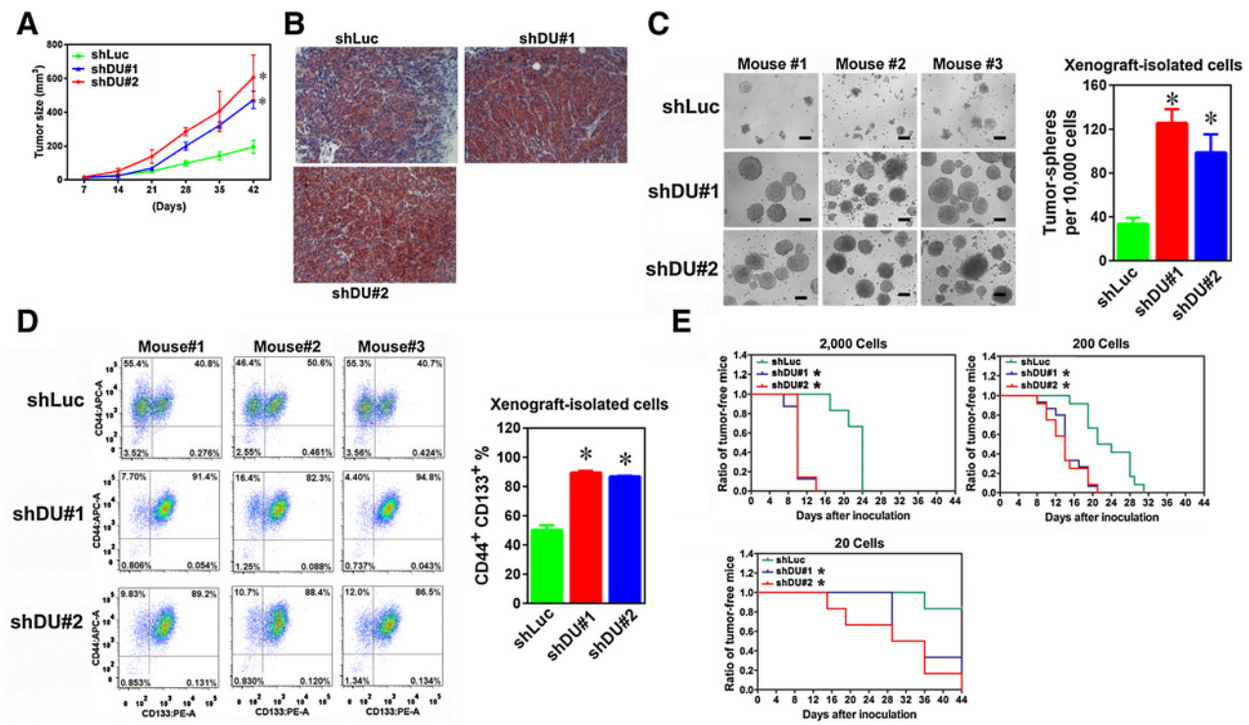

Figure 4.

Loss-of-DUSP2 promotes tumor growth and cancer stemness. **A,** Knockdown of DUSP2 in HCT116 cells (shDU#1 and shDU#2) promotes tumor growth in the xenografted mouse model. Each group contains four or five mice. *, significant difference compared with knockdown control (shLuc) at $P < 0.05$. **B,** IHC staining shows increased COX-2 expression in xenografted tumors grown from control (shLuc) and DUSP2-knockdown HCT116 cells. **C** and **D,** Number of tumorspheres and percentage of $CD44^{+/}CD133^{+}$ cell population and in cells isolated from xenografted tumors derived from control (shLuc) and DUSP2-knockdown (shDU#1 and shDU#2) HCT116 cells. Each experiment was individually repeated at least three times with cells isolated from 5, 5, and 4 mice. **E,** Tumor incidence of mice injected with different numbers of control (shLuc) or DUSP2-knockdown (shDU#1 and shDU#2) HCT116 cells.

Downloaded from http://aacrjournals.org/cancerres/article-pdf/77/16/4305/2753507/4305.pdf by guest on 26 August 2022

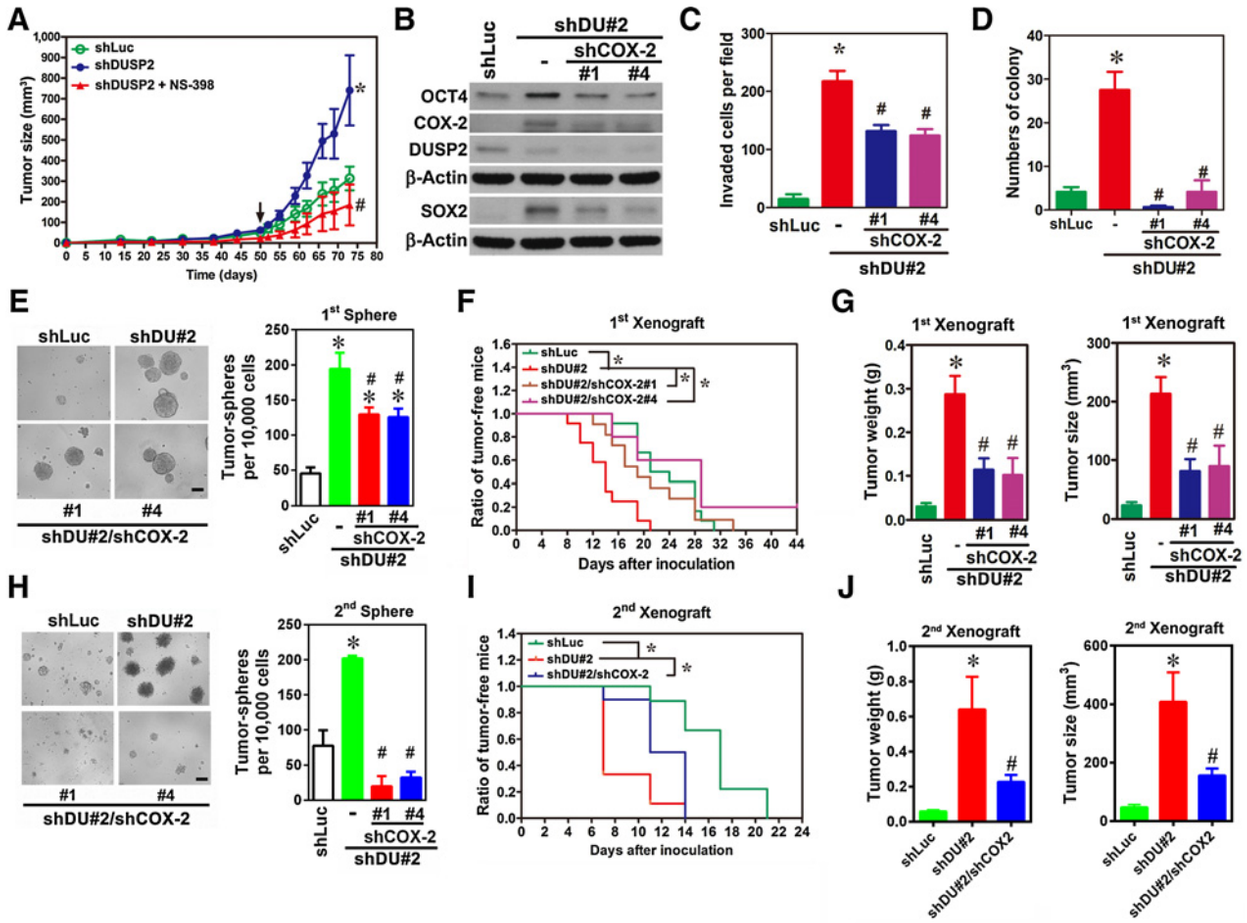

Figure 5.

COX-2 mediates loss-of-DUSP2-induced tumor growth and cancer stemness. **A,** Tumor growth curves of control cells (shLuc), DUSP2-knockdown (shDUSP2) cells, and DUSP2-knockdown cells treated with or without NS-398. After tumor reached 50 mm^3, 10 mg/mL NS-398 or vehicle was administered by intraperitoneal injection twice a week. Arrow, start of injection. **B,** Representative Western blots show levels of COX-2, DUSP2, OCT-4, SOX2, and β-actin in control (shLuc), DUSP2 knockdown (shDU#2), and DUSP2/COX-2 double knockdown (shDU#2/shCOX-2#1, shDU#2/shCOX-2#4) HCT116 cells. **C** and **D,** Invasion and anchorage-independent growth abilities of cells with knockdown control (shLuc), DUSP2 knockdown (shDU#2), and DUSP2/COX-2 double knockdown (shDU#2/shCOX-2#1, shDU#2/shCOX-2#4). **E–G,** Tumorsphere (**E**), tumor incidence (**F**), and tumor weights and sizes (**G**) of cells without (shLuc) or with DUSP2 knockdown (shDU#2) and DUSP2/COX-2 double knockdown (shDU#2/shCOX-2#1 and shDU#2/COX-2#4). **H–J,** Tumorspheres (**H**), tumor incidence (**I**), and tumor weights and sizes (**J**) of cancer cells isolated from xenografted tumors. Xenografted derived cells were injected into the back of mice for the second run of xenograft assay ($n = 6$ mice per group). *, $P < 0.05$ compared with respective controls; #, $P < 0.05$ compared with shDUSP2 only.

A (TSA), and valproic acid (VPA; Supplementary Fig. S6A) but not by class III HDACi (FK866 and Salermide, data not shown). Moreover, treatment with TSA, SAHA, and VPA significantly inhibited hypoxia-induced COX-2 expression (Fig. 6A). These data suggest that HDACs may be involved in hypoxia-induced DUSP2 downregulation and COX-2 upregulation. Indeed, knockdown of HDAC1 or HDAC2 reversed the hypoxia-mediated DUSP2 downregulation and COX-2 upregulation (Fig. 6B).

We then designed and synthesized novel HADCis, MPT0B369 (B369) and MPT0B390 (B390; Fig. 6C). Affinity assays showed that the IC_{50} levels of B369 and B390 for HADC1 were at least 5 and 10 times lower than that of SAHA while those for HADC2 were 6 and 15 times lower (Supplementary Table S6). Indeed, treatment with B369 and B390 exerted better effects in restoring DUSP2 levels and inhibiting COX-2 expression than SAHA (Fig. 6D–G). Consequently, treatment with B369 and B390 reduced the hypoxia-enhanced $CD44^+/CD133^+$ cell population, tumorsphere formation, and cell migration (Fig. 6H–K and Supplementary Fig. S6B). Moreover, treatment with B369 and B390 also inhibited basal and knockdown of DUSP2-induced tumorsphere formation (Supplementary Fig. S6C and S6D).

Xenograft experiments demonstrated that B369 and B390 significantly reduced tumor growth whereas SAHA failed to do so at the indicated doses (Fig. 7A and Supplementary S7A). The expression of COX-2 in xenografted tumor cells was also inhibited by treatment with B369 and B390 but not by SAHA (Fig. 7B). Combined treatment with B369 or B390 and known anticancer drugs, such as 5-fluorouracil, oxaliplatin (OXA), or paclitaxel, sensitized cancer cells to these drugs even under hypoxia (Fig. 7C and Supplementary Fig. S7B and S7C). As a result, combined

Downloaded from http://aacrjournals.org/cancerres/article-pdf/77/16/4305/2753507/4305.pdf by guest on 26 August 2022

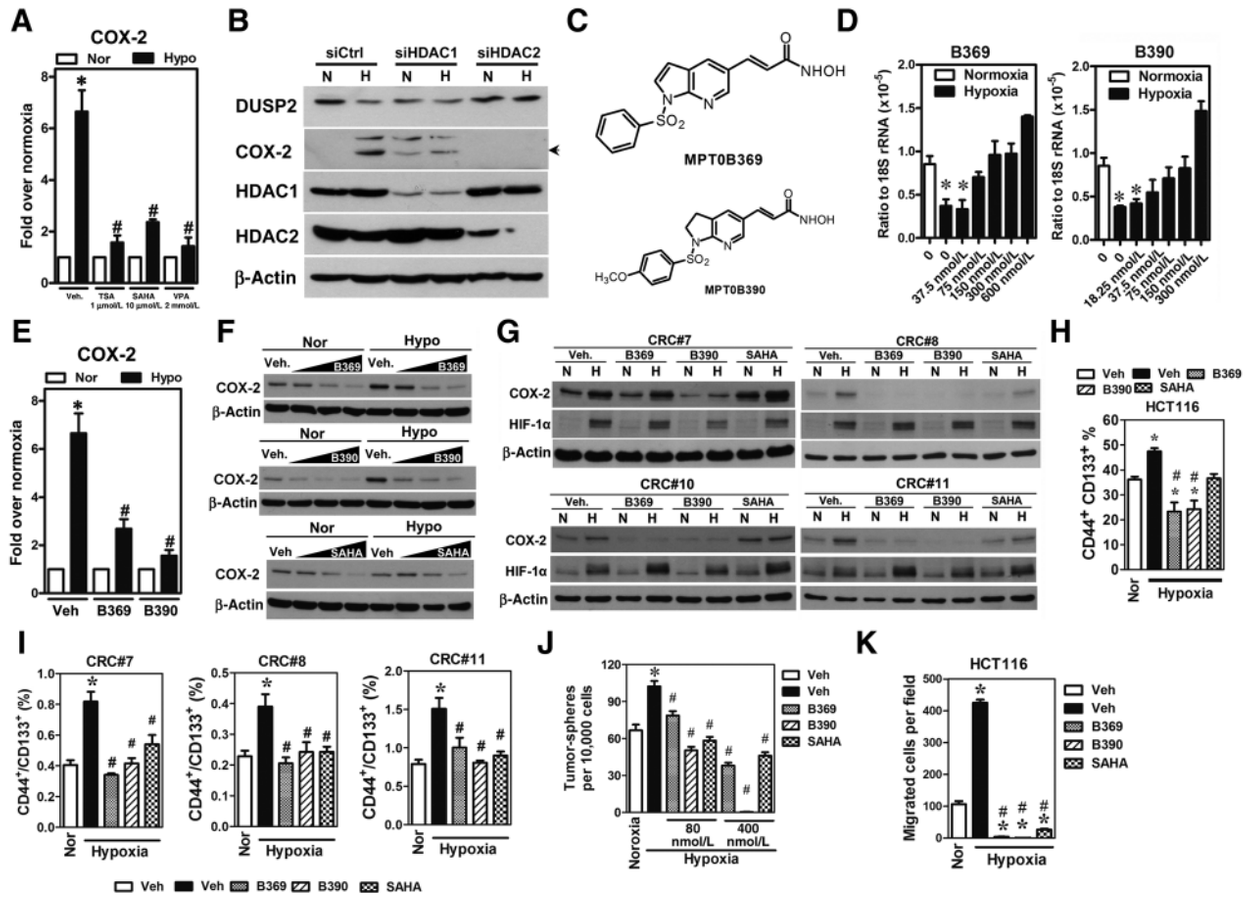

Figure 6.

Treatment with HDAC inhibitor abolishes hypoxia-induced COX-2 overexpression and cancer stemness. **A,** Treatment with HDACi ameliorates hypoxia (Hypo)-induced *COX-2* mRNA expression. *, $P < 0.05$ compared with normoxia (Nor); #, $P < 0.05$ compared with vehicle. **B,** Representative Western blots show levels of COX-2, DUSP2, HDAC-1, HDAC-2, and β-actin in HCT116 cells without (siCtrl) or with HDAC-1 (siHDAC-1) or HDAC-2 (siHDAC-2) knockdown. Arrows, COX-2 signal. The experiment was repeated three times using different batches of cells with similar result. **C,** Chemical structures of novel HDAC inhibitor. **D,** Levels of *DUSP2* mRNA in cells treated with different doses of MPT0B369 (B369) and MPT0B390 (B390) as indicated for 24 hours under normoxia or hypoxia. Data shown are the mean ± SEM of three independent experiments using different batches of cells; *, $P < 0.05$. **E,** Levels of *COX-2* mRNA in HCT116 cells cultured under normoxia or hypoxia in the absence (vehicle) or presence of novel HDACi (B369 and B390, 400 nmol/L) for 24 hours. *, $P < 0.05$ compared with normoxia; #, $P < 0.05$ compared with vehicle treatment under hypoxia. **F,** Inhibition of COX-2 protein by novel HDACi in HCT116 cancer cells. Cells were treated with MPT0B369 (B369), MPT0B390 (B390), or SAHA at the doses of 0.08, 0.4, and 2 μmol/L for 24 hours. **G,** Treatment with novel HDACi (400 nmol/L) abolishes hypoxia-induced COX-2 expression in primary colorectal cancer cells. *, $P < 0.05$ compared with normoxia; #, $P < 0.05$ compared with vehicle treatment under hypoxia. **H–J,** Treatment with novel HDACi (400 nmol/L) abolishes hypoxia-induced CSC cell population enrichment and tumorsphere formation. *, $P < 0.05$ compared with normoxia; #, $P < 0.05$ compared with vehicle treatment under hypoxia. **K,** Migration ability of HCT116 cells treated with vehicle (Veh), MPT0B369 (B369, 400 nmol/L), MPT0B390 (B390, 400 nmol/L), or SAHA (SAHA, 400 nmol/L). After treatment with HDACis under normoxia or hypoxia for 24 hours, cells were harvested for Transwell migration assay. Data shown are the mean ± SEM of three independent experiments using different batches of cells. *, $P < 0.05$ compared with normoxia; #, $P < 0.05$ compared with the hypoxia group treated with vehicle.

treatment with oxaliplatin and B369 or B390 exerted a synergistic effect in inhibiting tumor growth (Fig. 7D and E). Taken together, these data demonstrate that the novel HDACi, B369 and B390, can disrupt hypoxia-mediated, loss-of-DUSP2–dependent COX-2 overexpression and cancer stemness (Fig. 7F).

Discussion

CSCs are present in almost all types of cancer and are more resistant to conventional chemotherapies. Although there are articles describing the identification of CSCs in different types of cancer, the driving force for the enrichment of CSCs remains largely unknown. Herein, we demonstrated that hypoxia is a key factor behind the increased CSC population in several cancer cell lines and primary colorectal cancer cells. Hypoxia-mediated downregulation of DUSP2 leads to an increase in sensitivity of *COX-2* promoter and an overproduction of PGE_2. Because hypoxia is an inevitable consequence during cancer progression, our findings provide insights concerning the mechanism, which explain why COX-2 is constitutively activated in cancer cells. More importantly, we demonstrate that preventing DUSP2 from hypoxia-mediated downregulation or blocking loss-of-DUSP2–induced COX-2 overexpression is a feasible approach to disrupt hypoxia-induced cancer stemness.

Downloaded from http://aacrjournals.org/cancerres/article-pdf/77/16/4305/2753507/4305.pdf by guest on 26 August 2022

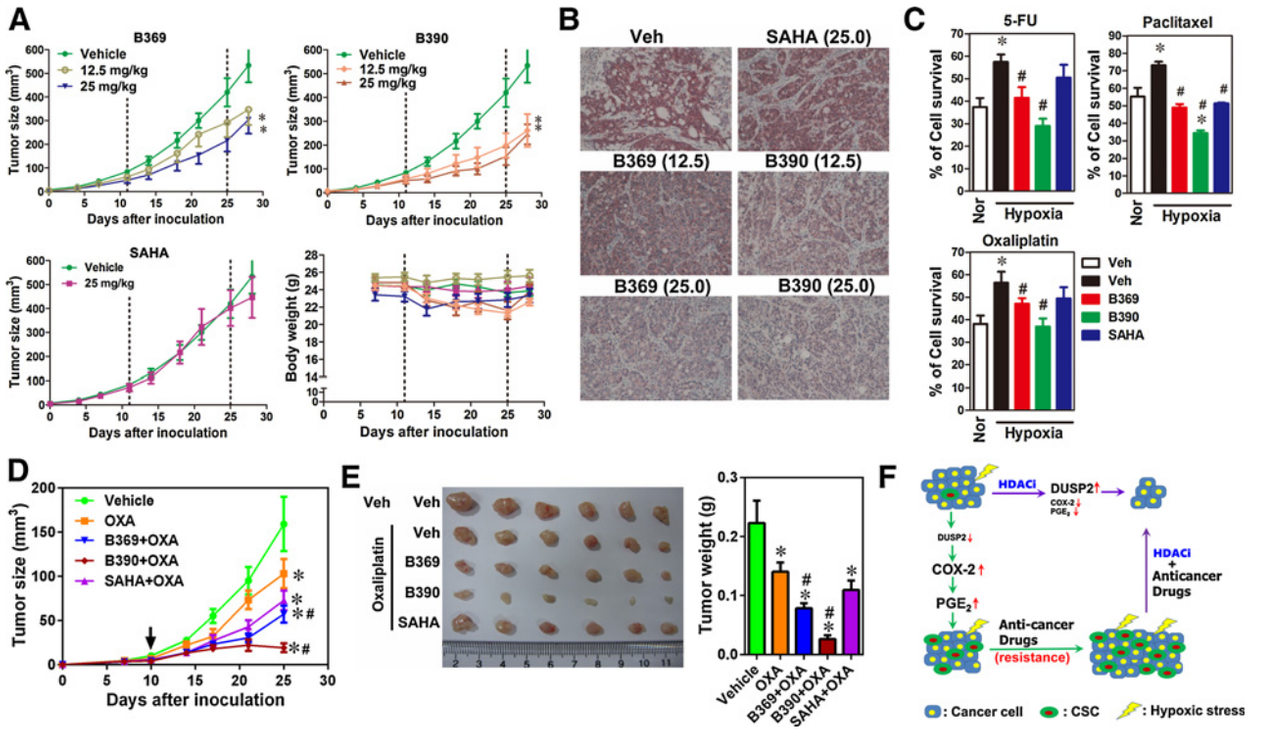

Figure 7.

HDACi inhibits tumor growth and reduces drug resistance. **A** and **B,** Treatment with B369 and B390 inhibits tumor growth and COX-2 expression in xenografted tumor. Drugs were administered orally between two dash lines. Note: the vehicle control group is the same set of data in different panels. *, $P < 0.05$ compared with the vehicle-treated group. **C,** Treatment with HDACi abolishes hypoxia-induced drug resistance. HCT116 cells were plated into 96-well for 24 hours and cotreated with 400 nmol/L HDACis and different kind of known anticancer drugs (2.5 μg/mL oxaliplatin, 160 μg/mL 5-FU, 25 μmol/L paclitaxel) for 48 hours. Each experiment was individually repeated at least three times. Nor, normoxia. *, $P < 0.05$ compared with normoxia; #, $P < 0.05$ compared with the vehicle-treated hypoxia group. **D,** HDACi effectively increases drug sensitivity in xenografted tumors. Arrow, date of treatments start. *, $P < 0.05$ compared with vehicle treatment; #, $P < 0.05$ compared with oxaliplatin (OXA; 10 mg/kg body-weight) treatment. **E,** Picture of xenografted tumor dissected from mice (left) and wet-weights of tumors (right). *, $P < 0.05$ compared with vehicle treatment; #, $P < 0.05$ compared with oxaliplatin treatment. **F,** Schematic drawing shows the working model of effects of novel HADCi on cancer intervention.

Dual specificity phosphatase-2 is a nuclear-specific MAPK phosphatase that regulates cell proliferation and apoptosis. Recent studies by our group and others revealed that DUSP2 is negatively associated with cancer malignancy (23, 29); however, the underlying mechanism remains unknown. Herein, we show that DUSP2 inversely controls cancer stemness. Our data demonstrate that suppression of DUSP2 by hypoxia markedly enriches the CSC population in cancer cell lines, primary colorectal cancer cells, and in xenografted mouse tumor. Forced expression of DUSP2 under a condition of hypoxia abolishes cancer stemness. Further study reveals that loss-of-DUSP2–induced cancer stemness is mediated by COX-2–derived PGE_2 production. Blockage of PGE_2 production or signaling markedly inhibits hypoxia and loss-of-DUSP2-induced cancer stemness and drug resistance. Our data agree with recent studies that treatment with PGE_2 promotes the CSC population whereas pharmacological inhibition of COX-2 activity by nonsteroidal anti-inflammatory drugs significantly decreases the numbers of tumorsphere (30–32). Furthermore, our data not only elucidate that the signaling pathway PGE_2 is used to promote cancer stemness, but also characterizes the most upstream cause, hypoxia, that leads to the aberrant production of PGE_2 during cancer progression.

Aberrant production of COX-2–derived PGE_2 in cancer cells has been known for several decades. However, the driving force initiating the aberrant expression of COX-2 in cancer cells remains largely unclear. In this study, by using a genome-wide screening approach, we identified that expression of COX-2 is negatively regulated by DUSP2. We demonstrated that hypoxia-mediated DUSP2 downregulation enhances *COX-2* promoter activity, which makes the *COX-2* promoter more sensitive to stimulation. As a result, not only do cancer cells tend to have a higher basal level of COX-2 but are also more vulnerable to stimulation by cytokines and growth factor presence in the tumor microenvironment. These proinflammatory cytokines and growth factors activate the *COX-2* gene expression in hypoxic cancer cells but not in normal cells because of the increased sensitivity of *COX-2* promoter to hypoxia. Our data demonstrate that the increase of *COX-2* promoter sensitivity is not directly contributed by the transactivation activity of HIF-1α since there was no detectable HIF-1α protein at the time of IL1β treatment. Instead, it is likely to be mediated by the pre-exposure of hypoxia, which suppresses DUSP2, as restoration of DUSP2 completely inhibits this synergistic effect.

To investigate the underlying mechanism responsible for the DUSP2-mediated increased *COX-2* sensitivity and to explore the potential of applying these findings in cancer intervention, we used a bioinformatic analysis using our microarray data and the online database, connectivity map. Surprisingly, we found that

Downloaded from http://aacrjournals.org/cancerres/article-pdf/77/16/4305/2753507/4305.pdf by guest on 26 August 2022

HDACi are potential drugs to reverse loss-of-DUSP2 effects, suggesting histone modification is involved. Indeed, treatment with SAHA, TSA, and VPA reverses hypoxia-mediated DUSP2 downregulation and COX-2 overexpression. Thus, we designed and synthesized novel HDACi, MTP0B369 and MTP0B390 (detailed biochemical profiles will be presented elsewhere). Results from *in vitro* and *in vivo* studies demonstrate that treatment with these HDACis reduces COX-2 expression, cancer stemness, tumor growth, and drug resistance. These data provide solid evidence to demonstrate that disrupting the hypoxia-regulated gene network by HDACi is a promising strategy to reduce cancer stemness and drug resistance. Because hypoxia is an inevitable consequence during cancer progression, preventing DUSP2 from hypoxia-mediated downregulation represents a reasonable choice to ameliorate hypoxia-induced cancer stemness and malignancy. Further study in characterizing the pharmacokinetics of these novel HDACis is now underway, and should provide valuable information for clinical application.

Disclosure of Potential Conflicts of Interest

Jing-Ping Liou has ownership interest (including patents) in substance patent. No potential conflicts of interest were disclosed by the other authors.

Authors' Contributions

Conception and design: P.-C. Hou, H.S. Sun, S.-J. Tsai
Development of methodology: H.S. Sun
Acquisition of data (provided animals, acquired and managed patients, provided facilities, etc.): S.-C. Lin, J.-C. Lee
Analysis and interpretation of data (e.g., statistical analysis, biostatistics, computational analysis): Y.-H. Li, S.-C. Lin, S.-C. Lin
Writing, review, and/or revision of the manuscript: P.-C. Hou, Y.-H. Li, S.-J. Tsai
Administrative, technical, or material support (i.e., reporting or organizing data, constructing databases): J.-Y. Chang
Study supervision: C.-C. Kuo, S.-J. Tsai
Other (collected clinical samples, analyzed, and supervised outcome of primary colon cancer cell studies): B.-W. Lin
Other (designed, synthesized HDAC inhibitor compounds, and supervised the drug treatment experiments): J.-P. Liou
Other (discovery of novel HDAC inhibitor compounds, and supervised the drug treatment experiments): C.-C. Kuo
Other (synthesis of chemical compounds): Y.-M. Liu

Acknowledgments

We thank Miss Yi-Hsuan Ya, Yi-Chen Tang, and Yen-Yu Lai for valuable technical supports.

Grant Support

This work was supported by National Research Program for Biopharmaceuticals (NSC 101-2325-B-006-017), National Health Research Institute (NHRI-EX-102-10244BI), and Top University grant of National Cheng Kung University (D103-35A17).

The costs of publication of this article were defrayed in part by the payment of page charges. This article must therefore be hereby marked *advertisement* in accordance with 18 U.S.C. Section 1734 solely to indicate this fact.

Received November 7, 2016; revised April 14, 2017; accepted June 14, 2017; published OnlineFirst June 26, 2017.

References

1. de Sousa EMF, Colak S, Buikhuisen J, Koster J, Cameron K, de Jong JH, et al. Methylation of cancer-stem-cell-associated Wnt target genes predicts poor prognosis in colorectal cancer patients. Cell Stem Cell 2011;9:476–85.
2. Abelson S, Shamai Y, Berger L, Shouval R, Skorecki K, Tzukerman M. Intratumoral heterogeneity in the self-renewal and tumorigenic differentiation of ovarian cancer. Stem Cells 2012;30:415–24.
3. Dontu G, Al-Hajj M, Abdallah WM, Clarke MF, Wicha MS. Stem cells in normal breast development and breast cancer. Cell Prolif 2003;36Suppl 1:59–72.
4. Du L, Wang H, He L, Zhang J, Ni B, Wang X, et al. CD44 is of functional importance for colorectal cancer stem cells. Clin Cancer Res 2008;14: 6751–60.
5. Li C, Heidt DG, Dalerba P, Burant CF, Zhang L, Adsay V, et al. Identification of pancreatic cancer stem cells. Cancer Res 2007;67:1030–7.
6. Visvader JE, Lindeman GJ. Cancer stem cells in solid tumours: accumulating evidence and unresolved questions. Nat Rev Cancer 2008; 8:755–68.
7. Xing F, Okuda H, Watabe M, Kobayashi A, Pai SK, Liu W, et al. Hypoxia-induced Jagged2 promotes breast cancer metastasis and self-renewal of cancer stem-like cells. Oncogene 2011;30:4075–86.
8. Reya T, Morrison SJ, Clarke MF, Weissman IL. Stem cells, cancer, and cancer stem cells. Nature 2001;414:105–11.
9. Herreros-Villanueva M, Zhang JS, Koenig A, Abel EV, Smyrk TC, Bamlet WR, et al. SOX2 promotes dedifferentiation and imparts stem cell-like features to pancreatic cancer cells. Oncogenesis 2013;2:e61.
10. Schwitalla S, Fingerle AA, Cammareri P, Nebelsiek T, Goktuna SI, Ziegler PK, et al. Intestinal tumorigenesis initiated by dedifferentiation and acquisition of stem-cell-like properties. Cell 2013;152:25–38.
11. Zhang H, Wu H, Zheng J, Yu P, Xu L, Jiang P, et al. Transforming growth factor beta1 signal is crucial for dedifferentiation of cancer cells to cancer stem cells in osteosarcoma. Stem Cells 2013;31:433–46.
12. Heddleston JM, Li Z, Lathia JD, Bao S, Hjelmeland AB, Rich JN. Hypoxia inducible factors in cancer stem cells. Br J Cancer 2010; 102:789–95.
13. Groebe K, Vaupel P. Evaluation of oxygen diffusion distances in human breast cancer xenografts using tumor-specific in vivo data: role of various mechanisms in the development of tumor hypoxia. Int J Radiat Oncol Biol Phys 1988;15:691–7.
14. Olive PL, Vikse C, Trotter MJ. Measurement of oxygen diffusion distance in tumor cubes using a fluorescent hypoxia probe. Int J Radiat Oncol Biol Phys 1992;22:397–402.
15. Jain RK. Normalization of tumor vasculature: an emerging concept in antiangiogenic therapy. Science 2005;307:58–62.
16. Wang YK, Zhu YL, Qiu FM, Zhang T, Chen ZG, Zheng S, et al. Activation of Akt and MAPK pathways enhances the tumorigenicity of $CD133^{+}$ primary colon cancer cells. Carcinogenesis 2010;31: 1376–80.
17. Armstrong L, Hughes O, Yung S, Hyslop L, Stewart R, Wappler I, et al. The role of PI3K/AKT, MAPK/ERK and NFkappabeta signalling in the maintenance of human embryonic stem cell pluripotency and viability highlighted by transcriptional profiling and functional analysis. Hum Mol Genet 2006;15:1894–913.
18. Owens DM, Keyse SM. Differential regulation of MAP kinase signalling by dual-specificity protein phosphatases. Oncogene 2007;26: 3203–13.
19. Yin Y, Liu Y-X, Jin YJ, Hall EJ, Barrett JC. PAC1 phosphatase is a transcription target of p53 in signalling apoptosis and growth suppression. Nature 2003;422:527–31.
20. Jeffrey KL, Brummer T, Rolph MS, Liu SM, Callejas NA, Grumont RJ, et al. Positive regulation of immune cell function and inflammatory responses by phosphatase PAC-1. Nat Immunol 2006;7: 274–83.
21. Hsiao KY, Chang N, Lin SC, Li YH, Wu MH. Inhibition of dual specificity phosphatase-2 by hypoxia promotes interleukin-8-mediated angiogenesis in endometriosis. Hum Reprod 2014;29:2747–55.
22. Lin SC, Wang CC, Wu MH, Yang SH, Li YH, Tsai SJ. Hypoxia-induced microRNA-20a expression increases ERK phosphorylation and angiogenic gene expression in endometriotic stromal cells. J Clin Endocrinol Metab 2012;97:E1515–23.

Downloaded from http://aacrjournals.org/cancerres/article-pdf/77/16/4305/2753507/4305.pdf by guest on 26 August 2022

23. Lin SC, Chien CW, Lee JC, Yeh YC, Hsu KF, Lai YY, et al. Suppression of dual-specificity phosphatase-2 by hypoxia increases chemoresistance and malignancy in human cancer cells. J Clin Invest 2011; 121:1905–16.
24. Chuang PC, Wu MH, Shoji Y, Tsai SJ. Downregulation of CD36 results in reduced phagocytic ability of peritoneal macrophages of women with endometriosis. J Pathol 2009;219:232–41.
25. Goessling W, North TE, Loewer S, Lord AM, Lee S, Stoick-Cooper CL, et al. Genetic interaction of PGE2 and Wnt signaling regulates developmental specification of stem cells and regeneration. Cell 2009;136:1136–47.
26. North TE, Goessling W, Walkley CR, Lengerke C, Kopani KR, Lord AM, et al. Prostaglandin E2 regulates vertebrate haematopoietic stem cell homeostasis. Nature 2007;447:1007–11.
27. Budinska E, Popovici V, Tejpar S, D'Ario G, Lapique N, Sikora KO, et al. Gene expression patterns unveil a new level of molecular heterogeneity in colorectal cancer. J Pathol 2013;231:63–76.
28. Lamb J, Crawford ED, Peck D, Modell JW, Blat IC, Wrobel MJ, et al. The Connectivity Map: using gene-expression signatures to connect small molecules, genes, and disease. Science 2006;313:1929–35.
29. Karakashev SV, Reginato MJ. Hypoxia/HIF1alpha induces lapatinib resistance in ERBB2-positive breast cancer cells via regulation of DUSP2. Oncotarget 2015;6:1967–80.
30. Kurtova AV, Xiao J, Mo Q, Pazhanisamy S, Krasnow R, Lerner SP, et al. Blocking PGE2-induced tumour repopulation abrogates bladder cancer chemoresistance. Nature 2015;517:209–13.
31. Moon CM, Kwon JH, Kim JS, Oh SH, Jin Lee K, Park JJ, et al. Nonsteroidal anti-inflammatory drugs suppress cancer stem cells via inhibiting PTGS2 (cyclooxygenase 2) and NOTCH/HES1 and activating PPARG in colorectal cancer. Int J Cancer 2014;134:519–29.
32. Li HJ, Reinhardt F, Herschman HR, Weinberg RA. Cancer-stimulated mesenchymal stem cells create a carcinoma stem cell niche via prostaglandin E2 signaling. Cancer Discov 2012;2:840–55.

Downloaded from http://aacrjournals.org/cancerres/article-pdf/77/16/4305/2753507/4305.pdf by guest on 26 August 2022